Journal of Photochemistry and Photobiology A: Chemistry 204 (2009) 183–190

Contents lists available at ScienceDirect

Journal of Photochemistry and Photobiology A: Chemistry

journal homepage: www.elsevier.com/locate/jphotochem

Titanium dioxide and composite metal/metal oxide titania thin films on glass: A comparative study of photocatalytic activity

Andreas Kafizas, Suela Kellici, Jawwad A. Darr, Ivan P. Parkin *

Department of Chemistry, University College London, 20 Gordon Street, London WC1H 0AJ, UK

ARTICLE INFO

Article history:
Received 18 February 2009
Received in revised form 17 March 2009
Accepted 24 March 2009
Available online 2 April 2009

PACS:
73.61.Ey

Keywords:
TiO_2
Photocatalysis
Formal quantum efficiency (FQE)
Composite
Thin film
Comparative

ABSTRACT

Titania and composite (Ag, Au, W) titania coatings were prepared on glass microscope slides *via* a sol–gel dip-coating method. The resulting coatings were characterised by X-ray diffraction, Raman, scanning electron microscopy (SEM), wavelength dispersive X-ray (WDX), Brunauer–Emmett–Teller (BET) surface area analysis, atomic force microscopy (AFM) and UV–visible absorption techniques. Photocatalytic activity of the coatings was determined by photomineralisation of stearic acid under 254, 365 nm and white light sources monitored by FT-IR spectroscopy. These activities at 254 and 365 nm light were represented as formal quantum efficiencies (FQEs) after determination of photon flux. Water contact angle measurements were made before and after irradiation with monochromatic 254 or 365 nm light; all films demonstrated photo-assisted super hydrophilicity (PSH). A Ag:Au titania composite coating was found to be the most significant photoactive film. The mode of improved photocatalytic activity was postulated in terms of a charge separation model. The Ag:Au TiO_2 coating showed potential as a useful coating for hard self-cleaning surfaces due to its robustness, stability to cleaning and reuse and its photoactive response to indoor lighting conditions.

1. Introduction

Interest in titanium dioxide as a semiconductor photocatalyst has grown rapidly in recent years [1]. The inexpensive and easily obtainable compound's inherent ability to photoactivate reactions, whilst retaining its chemical inertness, has led to a global spark of interest into several applications [2]. The bulk of research has predominantly featured TiO_2 as a photocatalyst in the oxidation of organic pollutants [3]. However, the use of TiO_2 as a photocatalyst in the destruction of bacteria, cancer cells and viruses has recently received great attention [4–12,6,13–21]. Such research has led to the production of environmental, self-cleaning, photocatalytic technologies such as the "Hydrotect Tile" [22] and Pilkington Activ™ Glass [23].

TiO_2 has the ability to degrade organic material on its surface *via* photocatalysis in the presence of UV-light ($\lambda < 385$ nm) and an oxygen source (e.g., O_2/H_2O). All such photocatalysis reactions involve an initial photoexcitation process on the TiO_2 catalyst substrate where the photoexcited catalyst then interacts, on contact, with the ground state organic absorbate molecule. Activation of TiO_2 semiconductors requires photons with energy greater than its band-gap energy (E_{bg}) which falls within the UV-light range of the electromagnetic spectrum. If TiO_2 is photoexcited in the presence of O_2, it is widely accepted that hydroxyl ($OH^{\bullet}$) radicals are produced by photogenerated holes (h(+)) [1]. Hydroxyl radicals are highly reactive towards organic materials and have a primary role in the degradation process.

The overall process can therefore be summarised by the following equation:

$$\text{Organic} + [\text{O source}] \xrightarrow[\text{Air, Light} \geq E_{bg}]{TiO_2\ \text{semiconductor,}} CO_2 + H_2O + \text{Mineral acids} \quad (1)$$

Much of the recent research on TiO_2 utilised either stearic acid or methylene blue as an organic standard to test its photocatalytic activity [1]. However, most research groups represent photocatalytic data in their reports in such a way that they are usually incomparable to one another (i.e., normalised). Therefore, when it is stated that a given dopant metal/metal oxide enhances the photocatalytic activity of TiO_2, it is usually difficult to know quantitatively by how much unless it is presented as a formal quantum efficiency (FQE) where:

$$\text{FQE} = \frac{\text{rate of reaction(molecules degraded/cm}^{-2}\,\text{s}^{-1})}{\text{incident photon flux (photon cm}^{-2}\,\text{s}^{-1})} \quad (2)$$

* Corresponding author. Tel.: +44 20 7679 4669; fax: +44 20 7679 7463.
E-mail address: i.p.parkin@ucl.ac.uk (I.P. Parkin).

1010-6030/$ – see front matter © 2009 Elsevier B.V. All rights reserved.
doi:10.1016/j.jphotochem.2009.03.017

Calculations of FQEs are somewhat tedious as the photon flux of the lamp used must be determined by chemical actinometry.

Most TiO_2 semiconductors are produced *via* either a sol–gel or Chemical Vapour Deposition (CVD) processes [24]. This study focuses solely on TiO_2 and metal/metal oxide titania composite thin films that were synthesised by the sol–gel process. Several research groups have attempted to enhance the photocatalytic activity of TiO_2 by introducing dopant metals into a TiO_2 matrix to form a solid solution or to form a composite MO_x/TiO_2 [12,25–27]. It has been shown through comparative studies that the introduction of Ag or W into titania matrices results in an enhancement compared with an anatase standard where 10%Ag:Ti and 2%W:Ti (M%) composite formation leads to the greatest overall photocatalytic enhancements [12,28].

SEM imaging of the Ag doped TiO_2 films displayed nanocluster islands with a high silver density [12]. It was concluded that these islands acted as charge separators that could also provide an additional electron source to the host TiO_2 matrix due to their relatively high electron density. By donating extra electrons to the conduction band of TiO_2, more reactive species at the catalyst surface could be produced. It was also proposed that these islands could reduce electron–hole recombination *via* charge separation, promoting the formation of supplementary hydroxyl radicals and hence enhancing photoactivity. It can therefore be postulated that greater photocatalytic activities could be achieved upon doping titania films with superior charge separators. In light of this theory, insertion of more highly conducting particles, such as Au, within a titania matrix can invoke a greater overall photocatalytic enhancement.

X-ray diffraction studies of W doped TiO_2 films confirmed the presence of a separate WO_3 phase within the host medium [28]. Due to the differing conduction band energies of WO_3 and TiO_2, it was proposed that these discrete phases could act as charge separators. Hence if the TiO_2 host is optically excited, the lower lying conduction band of WO_3 could allow for electron transfer. This leads to an accumulation of electron–holes in the valence band of TiO_2 and also hinders bulk recombination leading to an increase in the formation of surface reactive species, therefore explaining the enhanced photoactivity.

In this paper, gold particles were incorporated into a titania matrix *via* two methods and both film types were analysed for improvements as photocatalysts. A series of films were also synthesised and compared closely to that of Au doped films. Investigation into the doping of Ag in conjunction with W or Au nanoparticles into titania films is also explored. The possibility of a reduction in band-gap was studied for all films. A thorough analysis of the photocatalytic activities was determined *via* the degradation of stearic acid under a 254 nm (UVC) lamp, a 365 nm (UVA) lamp and under a typical hospital light source and compared with results attained from an anatase standard. FQEs were quoted for the experiments performed under 254 and 365 nm light.

2. Material and methods

With the exception of tungsten(V) ethoxide, 95% that was purchased from Alfa-Aesar, all chemicals used in this investigation were purchased from Sigma–Aldrich Chemical Co; propan-2-ol, 99.5%; butan-1-ol, 99.8%; methanol, 99%; pentane-2,4-dione (acetylacetone), 99%; acetonitrile, 99%; silver nitrate, 99%; hydrogen tetrachloroaurate(III) hydrate (auric acid), 99.9%; ammonium citrate tribasic, 98%; titanium(IV) *n*-butoxide, 97%; potassium ferrioxalate, 99%; sulphuric acid, 98%; sodium acetate, 99%; 1,10-phenanthroline, 99%; stearic acid, methylene blue solution 1% w/v; low iron content microscope slides (VWR ISO 8037/1, 76 mm × 26 mm).

2.1. Sol–gel synthesis

2.1.1. Preparation of sols

TiO_2: Titanium-*n*-butoxide (17.08 g, 0.05 mol) was chelated with an acetylacetone (2.51 g, 0.025 mol)/butan-1-ol (32 cm^3, 0.35 mol) mixture forming a clear straw-yellow solution, with no precipitation. After an hour of stirring, distilled water (3.66 g, 0.2 mol) dissolved in propan-2-ol (9.04 g, 0.15 mol) was added to hydrolyse the titanium precursor. The solution was further stirred for an hour. Acetonitrile (1.66 g, 0.04 mol) was then added to the pale yellow solution and stirred for a final hour. This formed a clear straw-yellow colour without precipitate which was allowed to age overnight without stirring.

A range of TiO_2 films were made using gold and silver dopants. The naming of these films relates to the initial solution concentrations and the type of dopant, it does not refer to the actual amount of noble metal incorporated in the film that was often significantly lower (see Section 4).

1%Au:TiO_2: The procedure was identical to that for the TiO_2 sol except auric acid (0.1904 g, 0.00056 mol) dissolved in acetonitrile (3.11 g, 0.075 mol) was added to the sol an hour after the initial hydrolysis.

2%Au:TiO_2: Samples were made in an identical fashion and scale to the 1%Au:TiO_2 samples except twice the molar amount of auric acid was used (0.3927 g, 0.0012 mol).

Ag:TiO_2: Samples were made in identical fashion to the 1%Au:TiO_2 sample except silver nitrate (0.851 g, 0.005 mol) dissolved in acetonitrile (2.89 g, 0.07 mol) was added to the sol instead of the auric acid solution.

Nano-Au:TiO_2: Titanium-*n*-butoxide (17.03 g, 0.05 mol) was chelated with an acetylacetone (2.62 g, 0.025 mol)/butan-1-ol (32 cm^3, 0.35 mol) mixture forming a clear straw-yellow solution, with no precipitation and then stirred for an hour. Auric acid (0.2063 g, 0.0006 mol) was dissolved in distilled water (25 cm^3) and tribasic ammonium citrate (0.30 g, 0.0012 mol) separately dissolved in distilled water (25 cm^3). An aliquot (1.0 cm^3) of the gold solution was extracted and added to warm (≈60 °C) distilled water (17 cm^3). After boiling, an aliquot (2.0 cm^3) of the citrate solution was also extracted and added dropwise to the solution over a 1-min period. The golden solution turned from clear, to blue, to red—forming a nanoparticle suspension. After a further 2 min of heating, the suspension was allowed to cool to room temperature. An aliquot (3.0 cm^3) of the suspension was dissolved in propan-2-ol (9.03 g, 0.15 mol) and added to hydrolyse the titanium precursor. The solution remained a clear straw-yellow colour with no ppt and was stirred for a further hour. Acetonitrile (4.03 g, 0.10 mol) was then added to the pale yellow solution and stirred for a final hour, remaining a clear straw-yellow colour without precipitate and allowed to age overnight without stirring.

Nano-Au:Ag:TiO_2: The same procedure was adopted as in the nano-Au TiO_2 synthesis except silver nitrate (0.852 g, 0.005 mol) dissolved in acetonitrile (2.89 g, 0.07 mol) was added to the sol prior to stirring overnight.

W:TiO_2: The same procedure was adopted as in the TiO_2 sol preparation except tungsten(V) ethoxide (0.4203 g, 0.0010 mol) was added to the initial solution.

W:Ag:TiO_2: The same procedure was adopted as for the W:TiO_2 synthesis save silver nitrate (0.860 g, 0.005 mol) dissolved in acetonitrile (3.27 g, 0.08 mol) was added to the sol prior to stirring overnight.

2.1.2. Dip coating

For dip coating, the sols were transferred to tall narrow beakers in order to ensure that most of the slide could be immersed in the sol. Single-coat films were made on either glass microscope slides or quartz. Quartz glass cuts (≈20 mm × 20 mm × 4 mm) were

washed in methanol and microscope slides were washed in distilled water and subsequently rinsed with propan-2-ol. Both substrates were allowed to air dry for 2 h before use. The glass substrates were immersed in the sol by a locally constructed dipping machine and withdrawn at a steady rate of 0.2 cm s^{-1} to create a uniform double-sided single-coat. The quartz substrates were withdrawn more slowly (0.02 cm s^{-1}) to achieve thicker films. Approximately 15 duplicates were made on glass and 1–4 copies on quartz for each film type.

2.1.3. Calcination

All dip-coated substrates were calcinated in an oven from 25 °C (at a rate of 10 °C/min) to 500 °C, held at this temperature for 1 h and then allowed to cool to room temperature in the dark overnight.

2.2. Film characterisation

The samples annealed on glass microscope slide substrates were used for the characterisation of the films unless otherwise stated.

Field emission scanning electron microscopy (SEM) was performed on gold or carbon (for the samples that contained gold)-sputtered samples using a Jeol JSM-6301F; energy dispersive spectroscopy (EDX) was performed on carbon-sputtered samples using a Hitachi S570. Wavelength dispersive X-ray (WDX) analyses of carbon-sputtered samples were measured using a Philips ESEM and referenced against titanium, gold, silver and tungsten standards. Powder X-ray diffraction (XRD) patterns were measured on a Siemens D5000 diffractometer using monochromated Cu Kα radiation (λ = 1.5406 Å) in the reflection mode with glancing angle incidence over the range 10–70/2θ°. Raman spectra were acquired over the range 50–800 nm on a Renishaw Raman System 1000 using a helium–neon laser (λ = 632.8 nm) calibrated against the emission lines of neon. UV–visible absorption spectra of both the coatings on quartz and glass substrates were obtained using a Thermo Spectronic Helios Alpha single beam instrument over the range 300–800 nm. Hardness/scratch tests were conducted with a stainless steel spatula and diamond tipped pen. Adhesion measurements were made by the Scotch® tape test.

2.2.1. Surface topology

Brunauer–Emmett–Teller (BET) surface area measurements of the Ag:TiO_2, nano-Au:Ag:TiO_2, TiO_2 films and blank glass microscope slides were performed on a Micromeretics ASAP 2420 Accelerated Surface Area and Porosimetry System. Two films of each sample were taken and snapped into 32 roughly equivalent segments (≈6 mm × 13 mm sections) and then degassed at 150 °C in N_2 for 16 h prior to analysis.

Atomic force microscopy (AFM) was used to measure the surface topology and Rq roughness of the select Ag:TiO_2, nano-Au:Ag:TiO_2 and TiO_2 films on a Veeco Dimension 3100 system. All films were scanned for 5, 10 and 20 μm field sizes. The mean Rq roughness values were obtained.

2.2.2. Water droplet contact angle

Photoactive films often demonstrate photoinduced super hydrophilicity (PSH). This process involves the hydroxylation of the films surface upon UV-light stimulation. The degree of PSH can be assessed by observing the change in contact angle of a water droplet on the surface of a film after UV-illumination. Films were initially placed in the dark for a 3-day period, in order to reset any residual light activated PSH. A 1 μl droplet of distilled water was then carefully placed on the film surface and the diameter of the drop measured after settling. With knowledge of the volume and diameter of the water droplet, a simple trigonometric spreadsheet was used to calculate the contact angle of the water droplet. The water droplet was wiped from the surface and the sample placed under a 254 nm germicidal lamp (Vilber Lourmat 2 × 8W VL-208G-BDH/VWR Ltd.) a set distance of 93 mm from the lamp to sample for 1 h. Droplets were added and measured after every consecutive 1 h of illumination for a total of 4 h. Samples were once more placed in the dark for a 3-day period, the contact angle measurement process repeated, placed in the dark for another 3 days and then a final reading taken. The contact angle measurements were typically repeated five times on each sample at every time interval and an average value obtained. The data spread at any stage was actually very small typically less than 2°.

3. Theory/calculation

3.1. Photocatalytic activities

The photocatalytic activity of films was measured by the mineralisation of stearic acid, which has a low vapour pressure and is relatively easily oxidised. For these reasons it has become one of the most popular choices amongst researchers analysing photocatalytic activities.

The overall oxidation reaction corresponds to:

$$C_{17}H_{35}COOH + 26O_2 \xrightarrow[\text{Air, Light} \geq E_{bg}]{TiO_2/TiO_2\ \text{composite}} 18CO_2 + 18H_2O \quad (3)$$

Sample films were tested in triplicate after 3 days storage in the dark. The films were cleaned in propan-2-ol, oven dried in the dark at 70 °C for 1 h and coated with a stearic acid (0.02 M solution in methanol) layer *via* a spin coating technique [28]. A few drops of the solution were placed on the centre of the film surface, spun at 1000 rpm for 10 s and the process repeated twice more to obtain a dry, even coating. The films were once more oven dried at 70 °C for a further 1 h to ensure the solvent had evaporated. The photocatalytic activity of the films was monitored by Fourier transform-infrared (FT-IR) spectroscopy using a PerkinElmer RX-I instrument. The IR spectrum of each acid-over layer was recorded over the range 2980–2800 cm^{-1} and the areas of the peaks between 2950 and 2870 and 2870 and 2830 cm^{-1} integrated. These peaks respectively represent the C–H antisymmetric and symmetric stretches of stearic acid and can be directly related to the concentration of stearic acid on the film's surface [29]. The samples were irradiated using either a 254, 365 nm (Vilber Lourmat 2 × 8W VL-208BL-BDH/VWR Ltd., 230 V/50 Hz) or a white light source (GE lighting 2D fluorescent GR10q-835 white, 28W) at a set distance of 93 mm from the lamp to the sample for a given amount of time. The IR spectrum of each acid-over layer was then recorded over the same range 2980–2800 cm^{-1} and the peaks integrated in the same manner at each recess. This process was repeated for a total illumination time of 150 min for the 254 nm irradiated samples, 360 min for 365 nm samples and 3000 min for white light samples. Given that the mineralisation process was approximately zero order [24] a rate (molecules degraded/cm^{-2} s^{-1}) for each experiment was calculated. The mean of each triplicate experiment was taken, with the maximum deviation in the range as its associated error.

3.2. Actinometry

Ferrioxalate actinometry [30,31] was used to determine the photon flux (photon cm^{-2} s^{-1}) for both UV-lamps was calculated. As the photocatalytic rates and photon fluxes for the 254 and 365 nm lamp experiments were determined, this data was represented as a formal quantum efficiency (FQE).

4. Results and discussion

4.1. Synthesis

A variety of TiO_2 and composite Au, Ag and W:TiO_2 films were formed using a simple sol–gel method. The general principle behind this method is the hydrolysis of a titanium precursor and its subsequent polymerisation into a Ti–O–Ti network. The addition of a dopant metal (M) into the film can result in two types of films where either a uniform $Ti_xM_yO_2$ composite is formed or the dopant exists in a separate phase dispersed throughout the TiO_2 matrix. By dip coating, a thin layer of the titania precursor is deposited on the substrate where gelation of the sol is substantially accelerated compared to bulk systems [28]. Annealing of the samples in a furnace at 500 °C removes any trace solvent and enhances the packing of the Ti–O–Ti polymer system into a crystalline network. The films are chemically bonded to the surface of the glass by the dip-coat annealing process whereby the titanium centre reaction with surface bound hydroxyl groups to form a Si–O–Ti encourage to the surface.

The insertion of gold nanoparticles into the titania sol was achieved by two different synthetic approaches whereby either Au nanoparticles were made *via* Turkevich's method [32] and inserted during the hydrolysis stage or Au was pre-chelated with a coordinating solvent (acetonitrile) and inserted after the hydrolysis stage, forming nanoparticles *in situ*. The *in situ* approach was an adaptation of a synthesis developed by Parkin et al., also used in this study, for the formation of Ag doped TiO_2 films [12]. The mixing of tungsten ethoxide with the titanium-*n*-butoxide precursor allowed for tungsten insertion into the titania network during the polymerisation stage.

4.2. Physical characterisation

After annealing (500 °C), all films were completely resistant to peeling with Scotch ©tape or scratching with a stainless steel spatula, yet quite easily scratched with a diamond tipped pen. Repeated dipping of the films into distilled water had no effect on the coating's surface, which could not be wiped off. All films were optically transparent and of relatively uniform thickness, interference fringes due to slight variations in film thickness could just be seen upon movement of the substrate's position at the edges of the films.

The majority of the work reported here was achieved on glass microscope slides with no barrier layer. It is possible that elements from the glass particularly the alkaline components (Na, K, Ca) could diffuse into the films during annealing and reduce photocatalytic performance. However, we feel this did not occur to any measurable extent as we were never able to detect the alkali metals in the thin films by any of the characterisation tools used and when repeats were made on quartz glass we obtained equivalent analytical results and photocatalytic functional testing.

4.3. Characterisation

4.3.1. X-ray diffraction

X-ray diffractograms (XRD) of all films were indexed as predominantly anatase ($I4_1/amdz$, $a = 3.776$ Å, $c = 9.486$ Å) (Fig. 1). There was some evidence of a rutile component due to a small reflection observed at 27.4° in some samples. There were no detectable peaks relating to the presence of a separate dopant metal phase in any corresponding pattern. This could be attributed to the fact that the dopant metals/metal oxides were too low in concentration to be seen as a separate phase *via* XRD. The mean crystallite size of each material was determined by application of the Scherrer formula [33] to the most prominent anatase (1 0 1) peak using the CASA software suite [34] (Table 1). The percentage differences between

Table 1
Grouped photocatalysis, PSH, surface topology, optical, SEM thickness and crystallite size data for all the annealed films produced *via* a dip-coating sol–gel method on glass microscope slides.

Film	XRD	SEM	UV–vis	Surface topology		Water droplet contact angle		Photocatalysis		
	Crystallite size (nm)	Thickness (nm)	Band-gap (eV)	BET surface area ($m^2\ g^{-1}$)	AFM surface roughness RMS (nm)	>hydrophillic (before UV)	>superhydrophillic (after UV)	254 nm/ FQE $\times 10^{-3}$	365 nm/ FQE $\times 10^{-4}$	White light/molecules degraded/$cm^{-2}\ s^{-1} \times 10^{10}$
TiO_2	25 ± 3	90 ± 10	3.28 ± 0.12	0.172 ± 0.017	3.18 ± 0.29	53.7°	6.4°	2.65 ± 0.40	2.38 ± 1.19	2.50 ± 0.14
Nano-Au:TiO_2	25 ± 4	90 ± 10	3.18 ± 0.17	–	–	43.4°	2.7°	3.58 ± 0.25	9.43 ± 0.80	2.03 ± 0.15
1%Au:TiO_2	28 ± 7	100 ± 10	3.28 ± 0.10	–	–	80.0°	9.1°	4.07 ± 1.08	6.03 ± 2.22	1.66 ± 0.37
2%Au:TiO_2	25 ± 4	100 ± 10	3.18 ± 0.12	–	–	80.0°	9.1°	4.29 ± 2.34	5.03 ± 3.14	0.94 ± 0.11
Ag:TiO_2	28 ± 7	110 ± 10	3.15 ± 0.15	0.170 ± 0.017	1.63 ± 0.13	59.7°	3.5°	5.74 ± 1.06	3.28 ± 2.16	1.24 ± 0.75
Nano-Au:Ag:TiO_2	25 ± 4	90 ± 10	3.10 ± 0.25	0.188 ± 0.031	2.35 ± 0.87	59.7°	4.7°	2.83 ± 0.67	16.0 ± 1.41	3.57 ± 0.87
W:TiO_2	24 ± 4	110 ± 10	3.18 ± 0.08	–	–	35.0°	2.7°	3.13 ± 0.12	11.8 ± 0.58	2.26 ± 0.08
W:Ag:TiO_2	27 ± 2	100 ± 10	2.90 ± 0.10	–	–	43.4°	4.7°	3.26 ± 1.21	10.4 ± 1.32	2.25 ± 0.52

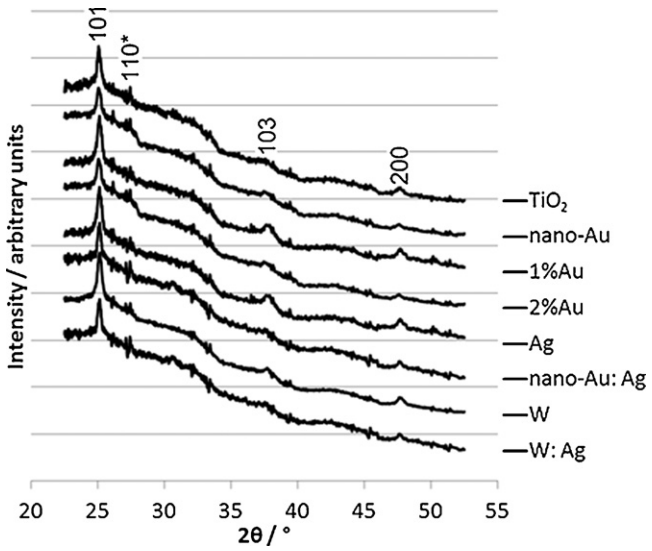

Fig. 1. Stacked XRD patterns for the annealed films produced *via* a dip-coating sol–gel method on glass microscope slides. The predominant phase observed was anatase TiO_2 (shown with Miller indices). Rutile TiO_2 reflections are shown by an *.

the true and modelled peak areas were used in estimating the associated error. All crystallite sizes were within error (24–28 nm), indicating no significant differences in crystallinity between all the samples.

4.3.2. Raman analysis

The Raman spectrum for the TiO_2 film showed a sharp and intense peak at 144 cm^{-1} and further peaks at 197, 320, 399, 515, and 519 cm^{-1}, directly attributable to anatase [35]. Smaller peaks displayed at 245, 357 and 560 cm^{-1} in some samples were attributed to rutile phases [36]; see Fig. 2. Comparisons of the peak intensities lead to the deduction that all films were predominantly anatase, which is in agreement with what was seen from XRD data. Broader and lesser defined Raman patterns were observed for *in situ* Au doped films compared with that of pure titania, where successively broader and lesser defined patterns were observed for the films with a higher composite fraction.

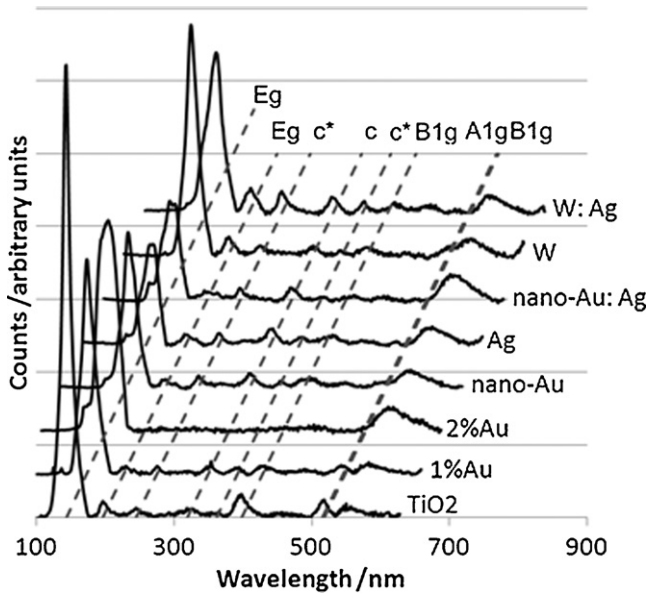

Fig. 2. Raman spectra of all the annealed films produced *via* a dip-coating sol–gel method on glass microscope slides ("c" denotes combination modes and the asterisk signifies modes attributable to rutile).

4.3.3. EDX, WDX and SEM analysis

EDX analysis of samples confirmed the presence of gold particles within the 1%Au, 2%Au, nano-Au and nano-Au:Ag:TiO_2 films. Wide area elemental analysis of the 1%Au and 2%Au:TiO_2 films showed no significant loss of gold from synthesis to product; however, the molar ratio of Au:Ti in the nano-Au doped films was 1:1000. Regardless of this, back-scattered SEM imaging on all carbon-sputtered samples displayed images with distributions of bright spots that close range elemental analysis confirmed to be areas of high gold density.

It can be seen that the size distribution of gold particles within the 1%Au and 2%Au doped film are relatively comparable, ranging from approximately 50 to 150 nm. Conversely, larger particles formed within the nano-Au and nano-Au:Ag films, ranging from approximately 0.5 to 1.5 μm. This difference in particle size can be attributed to the way in which gold was introduced into the starting sol. For the nano-Au films, the gold particles were preformed in water using citrate to limit particle growth and then added to hydrolyse the titanium precursor whereas the 1% and 2%Au films had gold particles formed *in situ* within acetonitrile, a coordinating solvent. The *in situ* method was significantly better in ensuring high Au levels in the films.

Upon viewing a series of back-scattered SEM images and with confirmation *via* elemental analysis, it was also observed that in both the 1% and 2%Au films, gold would tend to form larger particle agglomerates within film cracks that form upon annealing. An approximate factor of 10 difference in size was observed. Presumably these entrenched sites provided a lower energy for gold particle agglomeration than the surface.

WDX analysis confirmed the presence of gold, tungsten and silver within the corresponding films. Multiple spot analysis ($d = 1$ μm) across the surface of each film showed homogenous dispersions of the dopant metal(s). The percentage analysis of the 1% and 2%Au films were in agreement with previous EDX measurements; however gold within the nano-Au doped films could be detected but was at the detection limit of the instrument used (0.1 atom%). Hence in the transfer of gold from the nano-Au solution to the film was very poor and the nanoformed gold remains largely in the initial reactant solution and does not aggregate within the film possibly as the nanoparticles are charge stabilised and do not react directly with the titanium dioxide precursor. In the formation of either tungsten or silver containing films, a molar ratio of either 2%W/10%Ag:Ti was introduced to the starting sol for making the Ag, nano-Au:Ag, W, or W:Ag:TiO_2 films. WDX analysis of all tungsten and/or silver containing films gave W:Ti and Ag:Ti ratios of ≈1:100 parts in both cases. This related to an approximate 50% loss of tungsten and a 90% loss of silver from synthesis to product in all films.

SEM imaging showed similar morphologies for all coatings. Granular structures were observed surrounded by thin surface cracks that did not penetrate to the substrate (Fig. 3). Side on SEM studies yielded average thicknesses of ≈100 ± 10 nm.

4.3.4. BET surface area and AFM surface roughness

BET surface area measurements of three samples (TiO_2, Ag:TiO_2, nano-Au:Ag:TiO_2) on glass yielded low surface areas, all below 1 $m^2\ g^{-1}$. Measurements were run in duplicate, allowing a mean surface area and error range to be taken. All surface areas fell within their associated errors showing comparable surface areas within the portioned samples (Table 1). The measured surface areas were at the limit of the detection system used and should only be used as guide to show that the synthesised films had comparable surface areas and as common for dense oxide films the measured values

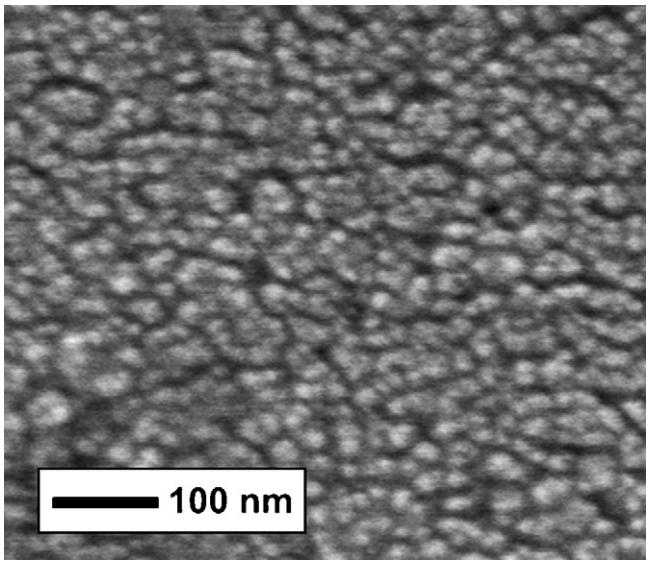

Fig. 3. An example image of the TiO_2 films surface attained *via* gold-sputtered sample SEM imaging; produced *via* a sol–gel method and annealed after dip coating onto glass.

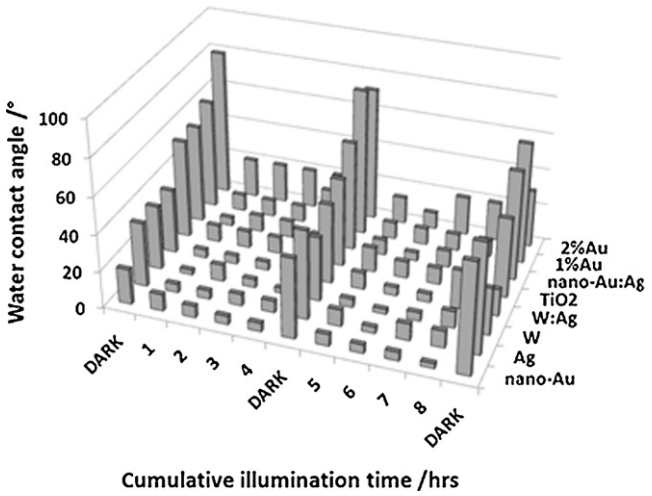

Fig. 4. A plot of water droplet contact angle (/°) versus cumulative 254 nm illumination time (h^{-1}) for all the annealed films produced *via* a dip-coating sol–gel method on glass microscope slides. DARK represents a 72 h period of film storage in complete darkness to reset the PSH mechanism.

were exceptionally low. Jung has measured the surface area of dense titania films from sol–gel and CVD and found values comparable with ours at 0.2 $m^2\ g^{-1}$ [36].

AFM analysis of the same three TiO_2, Ag:TiO_2 and nano-Au:Ag:TiO_2 samples yielded low RMS roughness values, all averaging orders of magnitude lower than 1 μm (Table 1). AFM imaging demonstrated the smooth topology of the films (see supplementary data). No trend in surface roughness was seen upon consecutive decreases in the field size of the analysis. The Ag:TiO_2 film displayed the lowest average roughness of 1.63 ± 0.13 nm and the TiO_2 film displayed the highest average roughness of 3.18 ± 0.29 nm. The nano-Au:Ag TiO_2 film did not significantly differ in surface roughness from either Ag:TiO_2 or TiO_2.

4.4. Functional properties

4.4.1. Water droplet contact angles

Initial water contact angle measurements showed that all films were relatively hydrophobic, making angles ranging from ≈44 to 80° depending on the coating. The measurement spread on any one surface was less than ca 2° over repeat measurements. Irradiation of the films with 254 nm caused a shift in contact angle towards hydrophilicity with contact angles in the range from ≈3 to 21° dependent on film, this is to be expected for titania films [1]. The lowest contact angle of 2.7° was measured on the W:TiO_2 sample that demonstrated superhydrophilicity [37]. All angles either remained constant or further decreased upon successive exposures to UV-light, with all films eventually displaying super hydrophilic contact angles (<10°). After a dark period, a reset towards hydrophobicity was seen for all films with increases in angles ranging from ≈44 to 73°. Subsequent re-exposures to UV radiation led to a replicable movement towards super hydrophilic contact angles for all films. A final dark period once again demonstrated a reset towards hydrophobicity, completing the PSH cycle (Fig. 4). The experiment was also repeated with 365 nm light and identical behaviour was observed.

4.4.2. Electronic spectra and band-gap energies

UV–visible absorption spectroscopy of all films over the range 300–800 nm displayed the O^{2-}–Ti^{4+} transition band edge minimum attributable to anatase [12]. Band-gap energies were calculated after extrapolating a Tauc plot [38] *via* manipulation of absorption data from thicker films on quartz substrates (Table 1). Due to the associated error in its calculation, merely the W:Ag:TiO_2 film could be said to have a significantly lowered band-gap to that of the pure titania film.

No evidence of a Ag surface plasmon resonance band was seen. It was quite viable the 500 °C annealing stage oxidised the Ag dopant to Ag_2O [39]; however there was no indication of this in the corresponding XRD pattern, most probably due to the low silver concentration within the titania film. Surface plasmon resonance bands relating to the presence of elemental Au nanoparticles were observed in the 1%Au and 2%Au doped films (quartz substrates), peaking at 634 nm on both occasions (Fig. 5), which is consistent given the oxidation resistance of Au [40]. The surface plasmon resonance of Au within a host matrix depends upon a variety of factors [41], the most important being the dielectric constant of the medium and particle size and shape. Assuming the particles are predominantly spherical, this resonance peak relates to particle diameters of ≈140–150 nm that fall within the range observed with back-scattered SEM imaging. A surface plasmon resonance band was observed, peaking at 528 nm, within the preformed nanocolloid suspension before insertion to sol in the synthesis of nano-Au doped films. Post-annealing, no nano-Au doped film

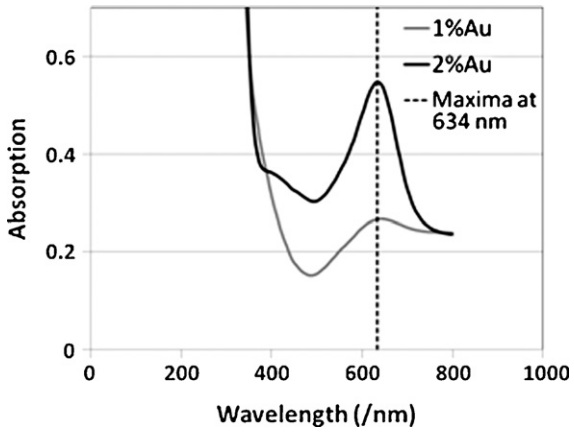

Fig. 5. UV–visible absorption spectra of both the 1% and 2%Au:TiO_2 films produced *via* a dip-coating sol–gel method on quartz microscope slides displaying a Au-surface plasmon resonance maxima at 634 nm red-shifted by the titanium dioxide medium.

displayed plasmon resonance. This was attributed to the low concentration of Au particles within the host matrix.

4.4.3. Photocatalytic activities

All films displayed photoactivity towards photomineralisation of a stearic acid layer under 254 nm ($(2.44 \pm 0.16) \times 10^{14}$ photon $cm^{-2}\,s^{-1}$), 365 nm ($(3.21 \pm 0.37) \times 10^{14}$ photon $cm^{-2}\,s^{-1}$) and white light (Table 1). The rates of stearic acid destruction reduced in the order 254 nm > 365 nm > white light for all samples. The corresponding energy of the 254 nm lamp (4.88 eV) far exceeds that of the calculated band-gap energy for the thin films. Energy from the 365 nm lamp (3.40 eV) falls on the O^{2-}–Ti^{4+} boundary (Table 1). The order of magnitude decrease in activity of films from 254 to 365 nm illumination indicated photon absorption of wavelengths near or at the boundary was not as effective at creating electronic excitation as wavelengths above the boundary. The white light source (the most common light source in UK hospitals) emits a range of radiation over mainly the visible, but also a miniscule portion in the UV (see supplementary data-peak at 405 nm). As only a fraction of photons have sufficient energy to cause electronic excitations, photocatalytic rates of orders of magnitude lower than both the 254 and 365 nm light tested samples were observed.

Any degradation of stearic acid was due to photocatalysis, as all control (stearic acid coated glass slide) samples tested against any light source showed no activity. The Ag:TiO_2 film was most active under 254 nm light ($(5.74 \pm 1.06) \times 10^{-3}$ molecules degraded/photon) showing a FQE more than double that of pure TiO_2. Although the 2%Au:TiO_2 film seemed to be the second most active under 254 nm light ($(4.29 \pm 2.34) \times 10^{-3}$ molecules degraded/photon), the varying rates observed over the three separate films of the same type created an associated error where no other rate seen fell outside this range. The doped films that fell outside the highest error, proved to be significantly more photoactive than TiO_2 were the nano-Au, 1%Au and 2%W doped films.

The distribution of FQEs changed extensively for 365 nm tests, with the nano-Au:Ag:TiO_2 film showing greatest activity with 365 nm light ($16.0 \pm 1.41 \times 10^{-4}$ molecules degraded/photon), approximately five times more active than the pure TiO_2 film. The W and W:Ag:TiO_2 films also displayed rates considerably higher than that of the pure titania film, with activities ≈3–4 times greater whereas the Ag:TiO_2 film that showed the highest rate under 254 nm illuminations now exhibited rates no different outside of significant error to that of pure titania. The distribution of rates attained from white light testing remained similar to those obtained from the 365 nm experiments. Only the titania standard opposed this trend, with a photocatalytic rate higher than all other doped coatings, save one, the nano-Au:Ag:TiO_2 film, which displayed a significantly higher rate of $3.57 \pm 0.87 \times 10^{10}$ molecules degraded/$cm^{-2}\,s^{-1}$. Although the W:Ag:TiO_2 film showed the greatest visible energy band-gap shift, a rate 1.6 times slower than the nano-Au:Ag:TiO_2 film was seen.

4.4.4. Internal comparisons and relationship to published data

The introduction of either W, Ag or Au (or combinations) as the metal (Au) or metal oxide into a titania medium did not show any evidence of a peak shift in their respective Raman or XRD patterns, suggesting the formation of composite films. UV–visible absorption profiles of 1% and 2%Au:TiO_2 films confirmed the presence of composite formation in these from the display of surface plasmon resonance and the observation of a secondary phase in the back-scattered SEM image. Interestingly there did not seem to be a direct correlation between FQE and degree of metal dopant within the titania films although the gold-doped titania films showed greater efficiency with white light at lower gold concentrations.

Table 2
A comparison of the literature FQEs against those obtained in this work for the annealed nano-Au, Ag and Ag/TiO_2 films produced *via* a dip-coating sol–gel method on glass microscope slides.

	Lamp wavelength	
	254 (nm)	365 (nm)
Coating	FQE (molecules degraded per incident photon)	
Pilkingtons Activ™ glass	3.06×10^{-4}	2.14×10^{-5}
P25 Degussa	7.83×10^{-3}	4.68×10^{-4}
Ag:TiO_2	$5.74 \pm 1.06 \times 10^{-3}$	$3.28 \pm 2.16 \times 10^{-4}$
Nano-Au:Ag:TiO_2	$2.83 \pm 0.67 \times 10^{-3}$	$16.0 \pm 1.41 \times 10^{-4}$

A photocatalytic study of stearic acid on Pilkingtons Activ™ and a very thick film of P25 Degussa TiO_2 made by a doctor blade technique (paste sample that was calcined; 70% anatase:30% rutile) was recently reported by Mills and co-workers [42]. Equivalent wavelengths were tested and rates quoted as FQEs allowing for analogous comparisons with the films made in this study (Table 2). The Pilkington Activ™ glass displayed the lowest rates of photocatalysis in both experiments due to the comparatively thinner TiO_2 coating on the glass substrate (25 nm thick). Under 254 nm, the nano-Au:Ag and Ag doped films reported here showed rates approximately 20 and 10 times greater than Pilkington Active™ respectively. Thick (10 μm) P25 Degussa was more active than all films made in this study at 254 nm showing rates 35% greater than the Ag doped film and 185% greater than the nano-Au:Ag doped film. This was attributed to its higher surface area, mixed rutile/anatase content and ≈100-fold increase in thickness compared with films reported here. However, under 365 nm light, the nano-Au:Ag doped film displayed significantly higher FQE rates, a factor of 75, 5 and 3.5 times more than Pilkington Activ™ glass, Ag doped titania and P25 Degussa respectively. Taking the experimental evidence seen here, as well as comparisons with literature, the nano-Au:Ag doped film made in this study displayed the greatest potential at 365 nm. We realise that this comparison does not take into account the relative thicknesses of the films or film crystallinity. However by using FQE as a benchmark method we are able to directly compare the "as formed" efficiency of the films in destroying stearic acid.

There are a number of avenues that can be followed in an attempt to provide an explanation for the enhanced activity of the nano-Au:Ag:TiO_2 film at longer wavelengths. Despite its relatively high band-gap (3.10 eV), the film's longer wavelength activity implied that it was efficient at generating reactive species with any UV photon. As no direct correlation between calculated band-gap and photoactivity was seen at any wavelength tested, a charge separation model was used to explain the activity enhancements [12,28]. Back-scattered electron SEM and EDX techniques confirmed Au and Ag existed within separate phases within titania. The separately doped nano-Au and Ag films did not show such an enhanced photocatalytic performance as the composite nano-Au:Ag:TiO_2 film, even though comparable dopant concentrations were observed *via* WDX analysis. The enhancement was therefore attributed to Au particles, working in conjunction with Ag, allowing for significantly greater charge transfer within the host matrix. This additional charge transfer would incur a more rapid generation of electron–holes and allow for the higher rates of photocatalysis observed. One aspect of this explanation that is difficult to reconcile is the fact that relative photoactivity of each sample type varied so markedly between 365 and 254 nm light illumination. Both the 254 and 365 nm light sources are significantly more energetic than the measured band-gaps and would be expected to have comparable photoactivities. This is obviously not the case, and suggests that the electron–hole pairs have different properties when generated by photons of different energy. This argument that spectral frequency can be correlated

with FQE has been forwarded previously by Serpone and Emiline [43].

The activity observed under hospital lighting conditions was somewhat surprising. The titanium dioxide film and the nano-Au:Ag:TiO_2 film showed the greatest activity. These films had two of the highest measured band-gaps. From this we conclude that the photoactivity observed in these experiments was due to the tiny fraction of UVA emitted from the hospital light source and not due to any form of visible light photoactivity.

5. Conclusion

A range of Au, Ag and W doped photocatalytically active coatings were synthesised by a simple sol–gel dip-coating method. The resultant coatings were characterised by glancing angle X-ray diffraction, Raman spectroscopy, SEM, EDX, WDX, BET, AFM and UV–vis spectroscopy. Films were shown to consist of titania predominantly in the anatase crystal form. All films demonstrated photoinduced super hydrophilicity (PSH) after subsequent exposure to UVC light, with contact angles as low as 2.7° observed. Photocatalytic activities of the coatings were characterised by the photomineralisation of stearic acid monitored by FT-IR spectroscopy under 254, 365 nm and white light sources. Actinometry was performed on both 254 and 365 nm light sources yielding photon fluxes allowing for formal quantum efficiency calculation. Coatings displayed greatest photocatalytic activities against both stearic acid at 254 nm, and progressively lower activities at higher wavelengths. It was found that the gold nanoparticle: silver(I) oxide doped titania films (nano-Au:Ag:TiO_2) exhibited significantly higher rates of photocatalysis at higher wavelengths than all others in this study, showing a firm trend towards visible light enhanced activities despite it's relatively high band-gap (3.10 eV). As no direct correlation between calculated band-gap and photoactivity was seen at any wavelength tested, a charge separation model was used to describe the mechanism by which this enhanced photoactivity was achieved. The nano-Au:Ag doped films showed the greatest potential for self-cleaning coatings due to their robustness, stability to cleaning and reuse and essentially, their visible light enhanced photocatalytic properties.

Acknowledgements

I.P.P wishes to thank the Royal Society and Wolfsen Trust for a merit award and express gratitude to Mr Kevin Reeves (UCL Archaeology) for assistance in SEM studies and Dr Steve Firth (UCL Chemistry) for his assistance in Raman spectroscopy studies.

Appendix A. Supplementary data

Supplementary data associated with this article can be found, in the online version, at doi:10.1016/j.jphotochem.2009.03.017.

References

[1] A. Mills, S. LeHunte, J. Photochem. Photobiol. A: Chem. 108 (1997) 1.
[2] Y. Katsunori, M. Ishikawa, Catal. Surv. Jpn. 4 (2000) 83.
[3] Web of Knowledge http://portal.isiknowledge.com, last accessed 8th January 2009.
[4] V. Keller, N. Keller, M.J. Ledoux, Chem. Commun. 1 (2005) 2918.
[5] T. Nonami, H. Hase, K. Funakoshi, Catal. Today 96 (2004) 113.
[6] W. Jacoby, P.C. Maness, E.J. Wolfrum, Environ. Sci. Tech. 32 (1998) 2650.
[7] T. Matsunaga, T. Nakajima, Appl. Environ. Microbiol. 50 (1985) 238.
[8] R.J. Watts, S.H. Kong, M.P. Orr, Water Res. 29 (1995) 95.
[9] T. Matsunaga, R. Tomoda, T. Nakajima, Appl. Environ. Microbiol. 54 (1988) 1330.
[10] J.C. Ireland, P. Klostermann, E.W. Rice, Appl. Environ. Microbiol. 59 (1993) 1668.
[11] Z. Huang, P.C. Maness, S. Smolinski, J. Photochem. Photobiol. A: Chem. 28 (1999) 1.
[12] I.P. Parkin, K. Page, R.G. Palgrave, J. Mater. Chem. 17 (2007) 95.
[13] K.P. Kuhn, I.F. Chaberny, K. Massholder, Chemosphere 53 (2003) 71.
[14] G.F. Fu, P.S. Vary, C.T. Lin, J. Phys. Chem. B 109 (2005) 8889.
[15] J.C. Yu, W.K. Ho, J. Lin, Environ. Sci. Tech. 37 (2003) 2296.
[16] G. Hyett, M.A. Green, I.P. Parkin, J. Am. Chem. Soc. 129 (2007) 15541.
[17] A. Rampaul, I.P. Parkin, L.P. Cramer, J. Photochem. Photobiol. A: Chem. 191 (2007) 138.
[18] G. Hyett, M.A. Green, I.P. Parkin, J. Am. Chem. Soc. 128 (2006) 12147.
[19] I.P. Parkin, R. Palgrave, J. Am. Chem. Soc. 128 (2006) 1587.
[20] I.P. Parkin, R. Palgrave, J. Mater. Chem. 15 (2005) 1689.
[21] S.A. O'Neill, R.J.H. Clark, I.P. Parkin, Chem. Mater. 15 (2003) 46.
[22] TOTO today http://www.toto.co.jp/en/abstract/today/pdf/04_0130today.pdf, last accessed 12th February 2009.
[23] Laminated Glass News http://www.dupont.com/safetyglass/lgn/stories/2208.html, last accessed 12th February 2009.
[24] A. Mills, G. Hill, S. Bhopal, I.P. Parkin, S.A. O'Neil, J. Photochem. Photobiol. A: Chem. 160 (2003) 185.
[25] S.D. Sharma, D. Singh, K.K. Saini, Catal. Appl. 314 (2006) 40.
[26] E. Celik, Z. Gokcen, N.F.A. Azem, Mater. Sci. Eng. B-Solid 132 (2006) 258.
[27] S.R. Sonawane, M.K. Dongare, J. Mol. Catal. A-Chem. 243 (2006) 68.
[28] I.P. Parkin, A. Rampaul, S.A. O'Neil, J. DeSouza, A. Mills, N. Elliott, Polyhedron 22 (2003) 35.
[29] A. Mills, M. McFarlane, Catal. Today 129 (2007) 28.
[30] C.A. Parker, P. Roy, Soc. Lond. A Mater. 220 (1953) 104.
[31] C.A. Parker, Trans. Faraday Soc. 50 (1954) 1213.
[32] J. Kimling, M. Maier, B. Okenve, V. Kotaidis, H. Ballot, A. Plech, J. Phys. Chem. B 110 (2006) 15700.
[33] A.L. Patterson, Phys. Rev. 56 (1939) 978.
[34] CASA software suite http://www.casaxps.com, last accessed 8th January 2009.
[35] S.J. Rigby, A.H.R. Al-Obaidi, S.K. Lee, D. McStay, P.K.J. Robertson, Appl. Surf. Sci. 252 (2006) 7948.
[36] S.C. Jung, Korean J. Chem. 25 (2008) 364.
[37] A. Marmur, Langmuir 20 (2004) 3517.
[38] B. von Blanckenhagen, D. Tonova, J. Ullmann, Appl. Opt. 41 (2002) 3137.
[39] P.K. Jain, X. Huang, I.H. El-Sayed, M.A. El-Sayad, Plasmonics 2 (2007) 107.
[40] Greenwood, Earnshaw, Chemistry of the Elements (2nd Edition), Butterworth-Heinemann Ltd., 1984, 961 & 983.
[41] R.G. Palgrave, I.P. Parkin, Chem. Mater. 19 (2007) 4639.
[42] I.P. Parkin, A. Mills, A. Lepre, J. Photochem. Photobiol. A: Chem. 160 (2003) 213.
[43] A.B. Emeline, N. Sepone, J. Phys. Chem. B 106 (2002) 2221.